Journal of ELECTRONIC MATERIALS, Vol. 46, No. 8, 2017
DOI: 10.1007/s11664-017-5462-4

Design and Characterization of the Ge/Ga_2S_3 Heterojunction

S.E. AL GARNI[1] and A.F. QASRAWI[2,3,4]

1.—Physics Department, Faculty of Science-Al Faisaliah, King Abdulaziz University, Jeddah, Saudi Arabia. 2.—Departments of Physics at AAUJ, Jenin and Group of Physics, Faculty of Engineering, Atilim University, 06836 Ankara, Turkey. 3.—e-mail: atef.qasrawi@atilim.edu.tr. 4.—e-mail:atef.qasrawi@aauj.edu

In this work, the formation and properties of Ga_2S_3 thin films deposited onto polycrystalline Ge substrates are studied by means of scanning electron microscopy, energy dispersive x-ray analyzer, Raman spectroscopy, x-ray diffraction techniques, ultraviolet–visible light spectrophotometry in the range of 300–1100 nm and by ac signal power spectroscopy in the range of 0.2–3.0 GHz. The first four techniques allowed the determining of the stoichiometry, the vibrational frequencies, the lattice parameters, the plane orientations, the strain and the defect density for the interface. In addition, it was observed that the Ge/Ga_2S_3 interface exhibited conduction and valence band offsets of 0.83 eV and 0.82 eV, respectively, and the real part of the dielectric spectra experimentally exhibited four resonance peaks centered at frequencies above 357 THz. Moreover, the computational analysis of the imaginary part of the dielectric constant via the Drude–Lorentz model has shown that the interface wave filtering properties are controlled by the electron–plasmon coupling with plasma frequencies in the range of 1.33–2.30 GHz. The drift mobility of electrons in this range was found to be 15.61 cm^2/Vs. The real ability of the interface to control wave propagation was confirmed with ac signals propagating tests. The plasmonic features of the interface nominate it for use in microwave cavities and as wireless terahertz receivers.

Key words: Ge substrate, Ga_2S_3, *p–n* junction, terahertz, plasmon devices

INTRODUCTION

Recently, interfacing narrow-wide energy band gap materials have attracted the attention of researchers owing to the smart properties that they reveal. A narrow gap material provides a potential well for electrons relative to the wide gap barrier, with a depth given by the conduction band offset. These types of interfaces are employed to overcome the problem of low photocatalytic efficiency which arises from the election–hole recombination and narrow photoresponse range.[1] The narrow–wide energy gap materials interfacing was also observed to increase the photocurrent generated in solar cells via the complementary absorption bands which can extend the light-harvesting range from visible to near-infrared regions.[2] Bands narrowing to 0.80 eV in polymer solar cells were achieved through the control of high molar absorptivity, suitable energy levels, high charge carrier mobility and high solubility in organic solvents.[3] In this approach, it has been shown that semiconducting polymers based on electron-donating units combined with strong electron-withdrawing units can possess preferable photovoltaic features.[4]

The use of Ge as a narrow band gap substrate for a device interfacing with wide energy band gap materials has shown smart properties presented by photovoltaic effects and microwave resonators. As an example, the Ge–boron nitrides interface[5] displayed selective microwave band stop filter features associated with resonant tunneling diode characteristics. The Ge/BN interfaces exhibited a resonant circuit with a peak-to-valley current ratio of 63. This device behaved as a microwave resonator with a notch frequency of 2.7 GHz. In addition, since the

(Received July 9, 2016; accepted March 17, 2017; published online March 31, 2017)

germanium exhibits a high hole mobility compared to common elemental and compound semiconductors, it is regarded as an ideal substrate for future CMOS capacitor production.[6] On the other hand, Ga_2S_3 is reported as a wide band gap thin film material exhibiting nonlinear optical properties that appear to be promising for terahertz application.[7]

One of the famous challenges in the design of the narrow–wide gap interfaces is the variation in the materials composition. For many systems, where the alloy composition is varied, the conduction and valence band offsets are constant fractions of the band gap difference.[8] At the interface formation, the Fermi level should be constant through the structure, the bands have to be flat at large distances from the interface, the band gap of each material has to be constant at the interface (they change abruptly as defined by the band offsets) and the band bending in the interface region is such that the region is electrically neutral overall and the electric displacement is continuous at the interface.[8]

Literature data concern information about the Ge and about the Ga_2S_3 heterojunction interfaces.[9,10] The relationship between composition, structure and crystallization behavior in the pseudo-ternary glass system, $(100 - x)(0.8GeS_2–0.2Ga_2S_3)–x$CsI, is reported to exhibit a compositional threshold of crystallization behavior located at 6–7 mol.% CsI content. The threshold of the crystallizations is achieved via the heat treatment studies.[11] The glass transition temperature of the glassy system is highly dependent on the compositional properties. Some structural motifs like $Ge(Ga)S_4$, S_2GeI_2, S_3GaI and $S_3Ga–GaS_3$ are observed to be constructed in the glass network.[10] The existence of these motifs in the structure of the glassy system greatly influences the conduction and valence band alignments which directly affect the band bending properties when employed as heterojunction devices. In another system,[10] uniform and crack-free cubic Ga_2S_3 thin films were synthesized on n-GaAs (111) substrates by the sulfurization process. The Ga_2S_3 surface was composed of nanoparticles smaller than 50 nm in diameter. The Ga_2S_3 nanoparticles, clustered into regular triangle structures that were hierarchically packaged on GaAs, effectively reduced the reflectance of GaAs. The photoluminescence x-ray photoemission studies on this system indicated the existence of acceptor-like defects and type-I heterojunction with a valence-band offset of 0.6 eV for the Ga_2S_3/GaAs heterostructure.[10]

Unfortunately, no data can be found about the Ge/Ga_2S_3 heterojunction system. For this reason, the compositional and thermodynamic stability conditions of the $(100 - x)(0.8GeS_2–0.2Ga_2S_3)–x$CsI glassy system and the optimizing of the large band offset of the Ga_2S_3/GaAs heterostructure are the motivation for exploring the physical properties and applications of the Ge/Ga_2S_3 interface. It seems a promising interface which can behave as a terahertz resonator being able to harmonically oscillate light waves in the spectral range of 270–1000 THz. The features of the interface will be subjected to structural, compositional, vibrational, optical and dielectric analysis to set the possible applications of this design.

EXPERIMENTAL

Both the germanium (from 99.999% metal bases; Alfa Aeser) and the Ga_2S_3 (99.99% powders; Alfa Aeser) thin films were deposited using the vacuum evaporation technique with the help of a VCM600 thermal evaporator at a vacuum pressure of 10^{-5} mbar. The glass substrates which were ultrasonically cleaned were kept at a temperature of 250°C to obtain high mobility *p*-type Ge.[9] The obtained Ge films were used as substrates to evaporate the Ga_2S_3. During the evaporation of Ga_2S_3 onto Ge, the Ge substrate temperature was kept at 25°C to prevent any possible modifications of the substrate properties. As determined by an optical interferometer and a thickness monitor, the Ge and Ga_2S_3 film thicknesses were 1.0 μm. The x-ray diffraction patterns for the Ge/Ga_2S_3 interface were recorded using a Rigako Utima IV x-ray diffraction (XRD) unit at a scanning speed of 0.1°/min. The surface morphology and composition was studied using scanning electron microscopy (SEM) with a Joel JSM 7600F instrument that has an energy dispersion x-ray (EDX) analyzer. The Raman signal was recorded with the help of a high-resolution micro-Raman spectrometer (Thermoscientific DXR). The optical transmittance and reflectance spectra were recorded in the range of 300–1100 nm with the help of an evolution 300 spectrophotometer that is equipped with VEEMAX II reflectometer. The ac signal power was provided by Agilent N9310A radio-frequency signal generator (9 kHz–3 GHz) and the output power was recorded with the help of a GSP-830 3.0 GHz spectrum analyzer.

RESULTS AND DISCUSSION

The designed Ge/Ga_2S_3 interface is subjected to compositional, morphological and structural analysis by means of EDX, SEM and XRD techniques. The EDX and SEM images for the Ge/Ga_2S_3 interface are shown in Fig. 1a and b, respectively. The EDX analysis was taken over a 4.0-μm scale of enlargement of an area that covers the Ge and Ga_2S_3 interfacing region. The statistical data of the atomic contents in the area which is shown as a rectangle in Fig. 1a reveal a Ga and Se atomic contents of 39.7% and 60.3%, respectively. The values correspond to a chemical formula of Ga_2S_3. When the same measurements were repeated for samples deposited onto glass instead of Ge, the resulting stoichiometric composition is mostly found to be Ga_2S_3.

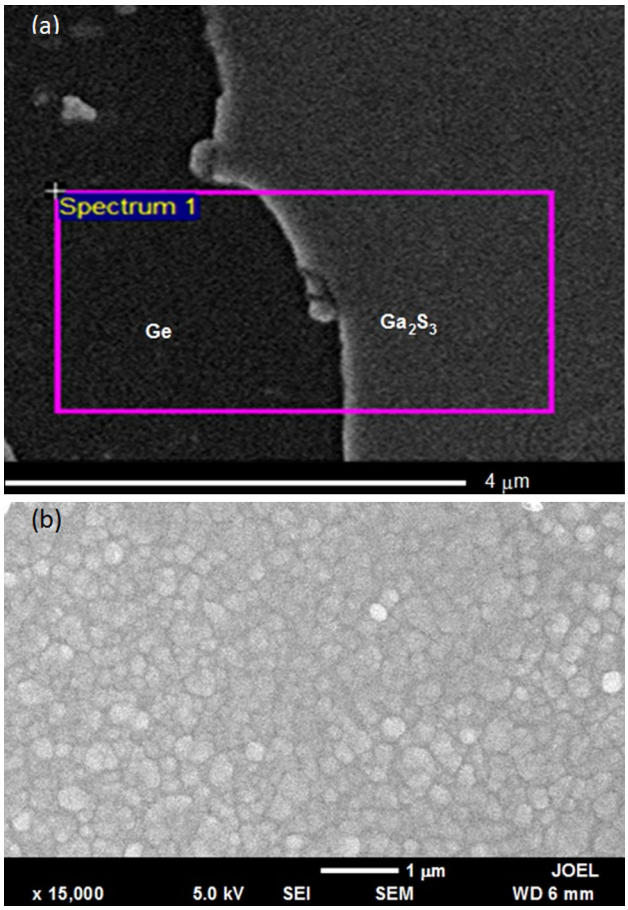

Fig. 1. (a) The SEM images for the Ge/Ga_2S_3 interface used in the EDX analysis and (b) an enlargement of 15,000 of the top surface (Ga_2S_3) of the interface which is shown in (a).

The SEM image shown in Fig. 1b was recorded from the top surface of the Ga_2S_3 thin films for an enlargement of ×15,000. As may be estimated from the image recorded from the Ga_2S_3 surface, an average grain size of 232 nm may be found with the help of the scale provided by the microscope.

To get more precise information about the formation of the Ga_2S_3 on the Ge substrates, the XRD for the Ge/Ga_2S_3 samples was recorded, as shown in Fig. 2a. The XRD patterns, which were analyzed with the help of software attached to the system, have shown that most of the intensive peaks refer to cubic Ge with preferable orientation (220). The reflections from the (111) planes are also very strong. The calculated cubic cell parameter was 5.65 Å that is in good relationship with earlier results for Ge.[9] In addition, some of the minor peaks are assigned to the cubic Ga_2S_3 and monoclinic α-Ga_2S_3 poly-phases.[10–12] The reflection peaks which appeared at $2\theta = 27.5°$ and at 53.9° can also be assigned to the monoclinic α-Ga_2S_3 (−312) and (−315) reflection planes, respectively (JCPDF cards of No. 84-1440).[10] One minor peak (18%) which appeared at $2\theta = 44.1°$ was assigned to the GeS compound. In the literature, the lattice parameter (a) for this cubic unit cell of Ga_2S_3 is reported to be 5.17 Å.[11] For the monoclinic α-Ga_2S_3 the cell parameters are $a = 11.094$, $b = 9.578$, $c = 6.395$ Å and $\gamma = 141°15'$.[12] Although the intensive peaks of x-rays for the Ge/Ga_2S_3 interface suggest a good lattice match between the cubic Ge and cubic Ga_2S_3 with very close values of cell parameters, it should be kept in mind that the Ga_2S_3 exhibits monoclinic, hexagonal and cubic crystal phases that appear at the same angles in the x-ray diffraction curves.[11,13] This behavior, which was assigned to the small distortions in the lattice structures between monoclinic and hexagonal Ga_2S_3,[10] make the exact identification of the structure hardly possible. On the other hand, the Ga_2S_3 thin films grown onto glass substrates in our laboratory are amorphous. Thus, the tendency of this material to exhibit a polycrystalline nature is due to the lattice match between the germanium substrate and the Ga_2S_3.

As mentioned above, the three structural phases can exist at the same diffraction angles. The significant difference between them appears in the change of the value of the relative intensity of the diffraction peaks, as observed for Ga_2S_3 deposited onto GaAs substrates.[13,14] Such a property indicates that even the monoclinic phase may be regarded as layered type with the wurtzite defective hexagonal in thin film form.[10–13] Since this type of crystallization is dominated by high vacancy disorder and because Ga_2S_3 is a naturally defect semiconductor with one-third of cation sites being vacant (Ga vacancies),[13] this kind of defect structure is easy to form an interfacial disorder of metal atoms in some specific interfaces. For these reasons, there is a need to obtain information about the defect density ($\delta = 15\epsilon/(aD)$[14]) which can exist in the interface of the composing materials. The microstrain ($\in$) of the Ge/Ga_2S_3 interface can be determined from the Stokes and Wilson expression for the strain broadening, $\beta\cos(\theta) = \frac{0.94\lambda}{D} + 4\epsilon\sin(\theta)$ with β being the peak broadening at full wave half maximum.[14] The slope of the $\beta\cos(\theta) - \sin(\theta)$ curves which is shown in Fig. 2b is negative value of 4.78×10^{-3} indicating that, for a cubic unit cell of lattice parameter of 5.65 Å, the unit cell is compressed by 2.7%. The compression in the unit cells is associated with a dislocation defect density of 2.15×10^{12} points/cm^2. The value of the defect density for the Ge/Ga_2S_3 interface is two orders of magnitude higher than those reported for Ge grown onto a Si substrate.[15] In reference to our EDX data, no Ge atoms are observed when data are collected from the surface of the heterojunction (Ga_2S_3 surface) and no Ga or S atoms are found on the surface of Ge at the interface junction. However, the appearance of the GeS as minor phases in the x-ray diffraction patterns indicates the possibility of the diffusion of some of the sulfur atoms into the Ge surface. Such an action could increase the defect density on the interface as

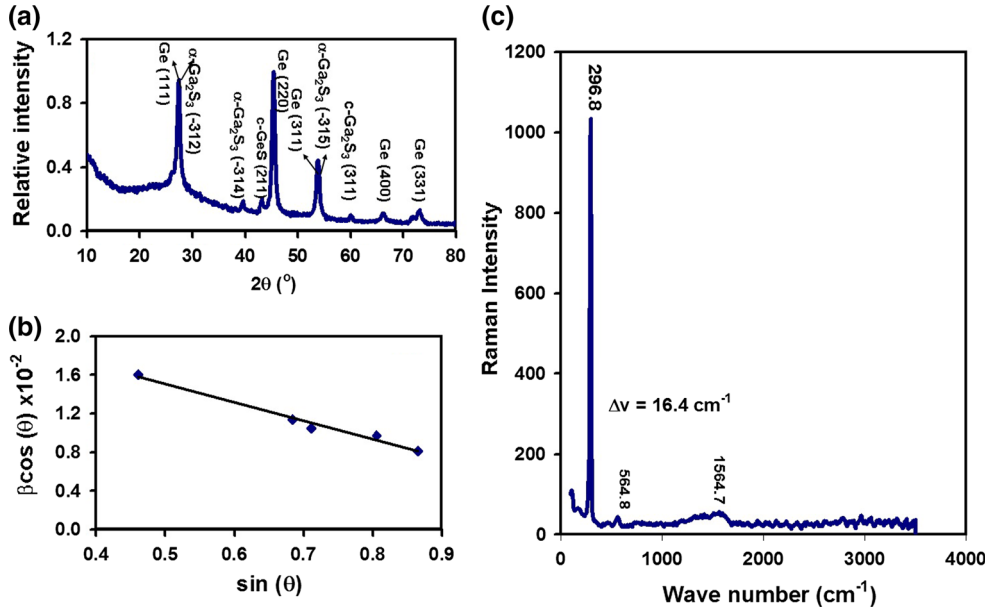

Fig. 2. (a) The XRD patterns, (b) the $\beta \cos(\theta) - \sin(\theta)$ variation and (c) the Raman spectroscopy of the Ge/Ga_2S_3 interface.

it leaves more S vacancies in the Ga_2S_3 structure. This prediction is consistent with that in Ga_2S_3/GaAs.[10] The low value of the compressing strain indicates that the large defects originated from the germanium surface (most of the x-ray peaks are assigned to the cubic Ge polycrystal). Similarly, the generation of dislocations in Ga_2S_3/GaAs heterostructure was previously assigned to both of the thickness increments of Ga_2S_3 and to the out diffusion of Ga atoms which can generate a defective region at the Ga_2S_3/GaAs interface or in the layer.[10]

The Raman spectra which were recorded for the interface using an exciting laser beam of 532.5 nm are shown in Fig. 2c. A very intensive narrow sharp line of full wave half maximum width of 16.4 cm^{-1} was detected at 296.8 cm^{-1}. The Raman spectra included other less intensive peaks centered at 564.8 cm^{-1} and 1564.7 cm^{-1}. The 296.8 cm^{-1} Raman shift refers to Ge crystalline phases.[16] Since the intensity of the peak is very high compared to the other minor peaks, the Ge substrates are regarded as exhibiting a high degree of crystallization. The observed Raman shift of Ge corresponds to a typical diamond structure (Ge-I) as reported in the literature, which confirms the x-ray results (Fig. 2a) which predict this type of structure.

It is also worth noting that the GaS crystal exhibits Raman active modes at 295 cm^{-1} and 296 cm^{-1} which belong to E^1_{2g} Raman active and to E_{1u} transverse optical vibration modes.[12] However, because the Raman spectra which are displayed in Fig. 2c are very sharp with a very narrow peak width which in turn indicate well-crystallized material, the probability of a Raman shift from 295 cm^{-1} to 296.8 cm^{-1} is excluded. To confirm this possibility, we tested the Ga_2S_3 films grown onto a cubic-structured Au substrate in the (111) orientation direction. The Raman spectra (not shown) of the Au/Ga_2S_3 did not reflect this strong peak which means that its only Ge-originated. The other two minor Raman active peaks which are observed at 564.8 cm^{-1} and 1564.7 cm^{-1} may be assigned to Ga vibrations as an impurity and as the C-O stretching of carboxylate ion bond which exists in the glass substrate, respectively.[17]

It is worth noting that different reactions at the Ge/Ga_2S_3 interface may also take place and should be thermodynamically considered and analyzed. Generally, to determine the stability of a compound under the thermodynamic equilibrium conditions, it is necessary to know the enthalpies of all possible decomposition reactions. If there exists a range of chemical potentials of pure elements within which all these enthalpies have positive values then within this range the formed compound is stable. For our design, under standard conditions, the condensation of gaseous Ga and S atoms onto the solid Ge element is associated with elemental chemical potentials (μ_i) 2.485 eV, 2.478 eV, and 3.494 eV[18] (Ge chemical potential is zero in solid form), respectively. Some of the possible chemical formations are GaS, Ga_2S_3, GeS and GeS_2. Practically, for the stable formation of Ga_2S_3, the following set of inequalities should be satisfied: $n\Delta\mu_X + m\Delta\mu_Y = \Delta H_f(X_nY_m)$, $\Delta\mu_I \le 0 (I = X, Y)$ and $n_i\Delta\mu_X + m_i\Delta\mu_Y \le \Delta H_f(X_{ni}Y_{mi})$. Here $\Delta\mu_I = \mu_i - \mu_i^{\mathrm{FERE}}$, is a deviation of the actual elemental chemical potential from its fitted elemental-phase reference energies (FERE) and Z is the total number of competing phases having $\Delta H_f(X_{ni}Y_{mi})$ enthalpies of formation.[19] The first of the inequalities (which is in fact equality) represents the thermodynamic

equilibrium condition between the compound and its elemental constituents and sets the allowed ranges of $\Delta\mu_I$ values. The published experimental data of ΔH_f for GaS, Ga_2S_3, GeS and GeS_2 are −1.09 eV, −1.07 eV, −0.39 eV and −0.66 eV, respectively.[19] The values of μ_i^{FERE} for Ga, S and Ge are −2.37 eV, −4.00 eV and −4.14 eV, respectively. The corresponding $\Delta\mu_I$ are −0.115 eV, −1.522 eV, and −1.560 eV, respectively. The second inequality is satisfied for the three elements. The left side of the first equality $n\Delta\mu_X + m\Delta\mu_Y = \Delta H_f(X_nY_m)$, exhibit values of −1.637 eV, −4.796 eV, −3.082 eV and −4.604 eV for GaS, Ga_2S_3, GeS and GeS_2, respectively. The numerical values show that the right hand side is not equal to the left hand side of the first inequality indicating that the thermodynamic equilibrium condition between the compounds and their elemental constituents are not satisfied unless the specific molar mass is included. The respective percentage ratios $\left(\frac{\Delta H_f(X_nY_m)}{n\Delta\mu_X+m\Delta\mu_Y}\right)$ of the two sides are 66.6%, 22.3%, 12.5% and 14.3%. However, because the second and third inequalities are also satisfied, it is possible to think that the formation of the GaS, Ga_2S_3, GeS and GeS_2 are stable[19] for the calculated molar ratios. As a result of these calculations, the most preferable formation refers to GaS followed by Ga_2S_3 on the top of Ge. On the other hand, studies of the glasses with stoichiometric compositions of $(100 - x)$ $GeS_{2-x}Ga_2S_3$, which were prepared by the melt-quenching technique, revealed that phase transformation behavior to form glasses containing Ga_2S_3 is the molar percentage of 14–15 mol.%.[20] In another system, the relationship between composition, structure and crystallization behavior in the pseudo-ternary glass system, $(100 - x)(0.8GeS_2–0.2Ga_2S_3)–x$CsI, is observed to exhibit a compositional threshold of crystallization behavior located at 6–7 mol.% CsI content.[10]

To reveal the application-directed properties of the heterojunction, we recall that the electron affinities of the Ge and Ga_2S_3 are 4.13[5] and 3.30 eV,[21] respectively. Thus, the conduction band offset (ΔE_c) is 0.83 eV. With this value of ΔE_c, there is a need to determine the shift in the energy band gap (ΔE_g) of the Ga_2S_3 upon Ge interfacing. For this reason, the absorption coefficient (α) spectra which were calculated from the transmittance (T) and reflectance (R) spectra are considered. The $\alpha - E$ dependence which is displayed in Fig. 3a exhibits very interesting characteristics presented by the very sharp decrease of the α-values in the incident light energy (E) region of 4.0–3.12 eV. The $\alpha - E$ variation follows strange characteristics in the region of 3.10–1.45 eV. Namely, the absorption coefficient increases with decreasing photon energy. The increasing trend is down reaching a minima at 2.57 eV and then re-increases reaching maxima at 1.47 eV, where it then tends to remain constant in the region of 1.46–1.08 eV. Figure 3a also displays the absorption coefficient spectra for the glass/Ga_2S_3 interface as a reference to the glass/Ge/Ga_2S_3 interface. The features of the absorption coefficient spectra of the Ga_2S_3 are also presented by a sharp fall of absorption coefficient values in the range of 3.70–2.62 eV. The latter spectra also exhibit two peaks centered at 2.33 eV and 1.47 eV. On the other hand, the direct energy band gap evaluation through the plotting of the $(\alpha E)^2 - E$ in

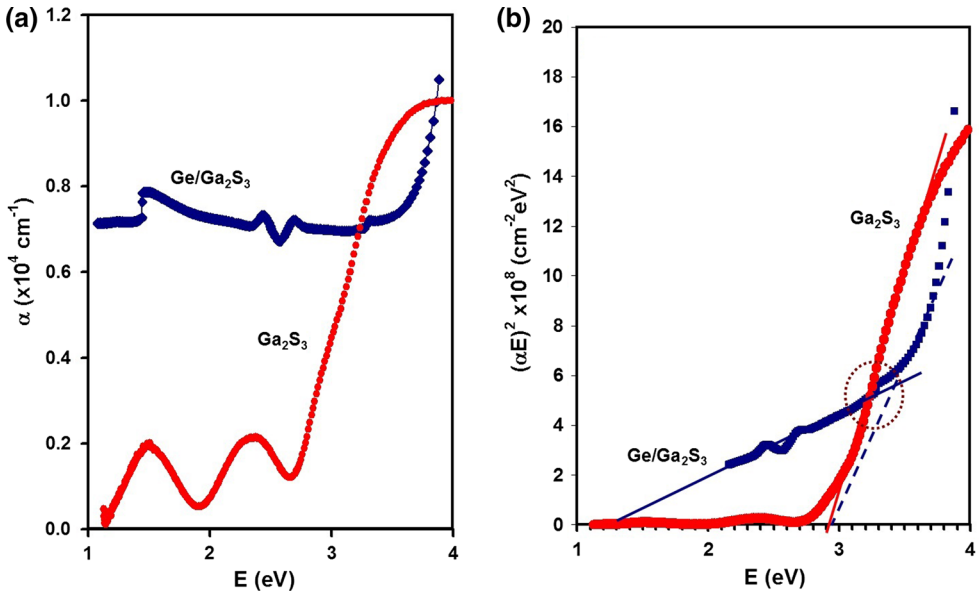

Fig. 3. (a) The absorption coefficient spectra and (b) $(\alpha E)^2 - E$ dependence for the glass/Ga_2S_3 and Ge/Ga_2S_3 interfaces.

accordance with the equation, $(\alpha E)^2 \propto (E - E_g)$ which is shown in Fig. 3b, reveals a direct allowed transitions energy band gap of 2.96 eV for Ga_2S_3 films, as shown by the solid and dashed blue lines in the figure, and an energy band gap of 1.85 eV for the Ge/Ga_2S_3 interface. The energy band gap of the Ge/Ga_2S_3 interface being 1.31 eV allows the determining of the valence band offset ΔE_v. The difference between the energy band gap of Ga_2S_3 and the energy band gap of Ge/Ga_2S_3 (ΔE_g) is 1.65 eV. Thus, the valence band offset is $|\Delta E_g - \Delta E_c| = 0.82$ eV.

The energy band gap of the Ga_2S_3 thin films reported here is consistent with that reported for Ga_2S_3 as 3.0 eV.[10–13] Studies on Ga_2S_3 using the photoluminescence, thermoreflectance, and optical absorption techniques have shown that this material exhibits three band-edge transitions, named E_A = 3.052 eV, E_B = 3.240 eV, and E_C = 3.328 eV. The E_A energy band transitions are assigned as the direct band gap of Ga_2S_3, and E_B and E_C are accepted to be exciton transitions near the band edge. The existence of these bands is attributed to the axial-dependent distribution of the p-states of the valence band. For the monoclinic phase of the α-Ga_2S_3, the highest valence band is shown to consist of mainly sulfur S($3p$) and some Ga($4p$) orbitals which are strongly oriented dump-bell-shaped bands.[13] On the other hand, the lowest conduction-band portion of α-Ga_2S_3 is mainly composed of Ga ($4s$) and some S($3p$) orbitals. Thus, the axial-dependent transitions from the lowest point of the conduction band to the tip of the dump-bell-shaped valence band will account for the E_A transition which is observed in this study. In addition, the valence band maxima of GeS in accordance with the electronic configuration of Ge and of S atoms should be mainly due to s-Ge, p_x, p_y-S and partially due to p_z-S. The two minima in the conduction band that could define the energy gap are mainly due to the p_x-Ge and p_y-Ge. These transitions display optical energy band gaps of ~1.10 eV and 1.21 eV, which are not observed in this work.[22]

Unfortunately, for possible comparison, information about the energy band transitions in the Ge/Ga_2S_3 heterojunction is not available in the literature. However, the valence band offset for this interface can be compared to other interfaces which are interfaced with germanium as substrates or top layers.[23] Numerical examples of these interfaces are listed in Table I. Such systems with these band offset execute a wide range of applications presented by thin film transistors,[6] photodiodes, microwave and terahertz resonators [5,7] and visible light communication devices.[24]

As one remarkable application, we have calculated the dielectric spectra from the measured specular reflectance (R) spectroscopic data which are displayed in Fig. 4a. The reflectance spectra of the Ge/Ga_2S_3 interface exhibit successive interference patterns which peak at 824 (3.39 eV), 714 (2.94 eV), 562 (2.31 eV) and 368 THz (1.51 eV). The last peak (368 nm) broadens to a wide range that extends from visible to infrared light range spectra (1.96–1.16 eV). These interference patterns should have arisen from interference between the incident waves and the waves reflected from the Ge and glass surface. However, the exact reasoning for the existence of these peaks at these incident photon wavelengths (energies) should be clearer in the forthcoming analysis which considers the modeling and details of the dielectric spectra. The effective dielectric constant (ε_{eff}) is determined from the relationship,[25]

$$R = \frac{\left(\sqrt{\varepsilon_{\text{eff}}} - 1\right)^2 + \left(\frac{\alpha\lambda}{4\pi}\right)^2}{\left(\sqrt{\varepsilon_{\text{eff}}} + 1\right)^2 + \left(\frac{\alpha\lambda}{4\pi}\right)^2}. \quad (1)$$

The effective dielectric constant is related to the real (ε_r) and imaginary (ε_{im}) parts of the dielectric constant through the relationships, $\varepsilon_r = \varepsilon_{\text{eff}} - \left(\frac{\alpha\lambda}{4\pi}\right)^2$ and, $\varepsilon_{\text{im}} = \sqrt{\varepsilon_{\text{eff}}}\left(\frac{\alpha\lambda}{2\pi}\right)$, respectively.[25] The relative plots of the real and imaginary parts of the dielectric spectra are displayed in Fig. 4b and c. Once again, sequence resonance peaks centered at 824 (3.39 eV), 715 (2.94 eV), 547 (2.25 eV), and 358 THz (1.47 eV) appeared in the real part of the dielectric spectra. The significance of these resonance peaks lay in the electronic transitions from the valence to the conduction bands of the Ga_2Se_3, while in accordance with the literature data, the 3.39 eV corresponds to the exciton transition in the α-Ga_2S_3 polytype which exhibits a band gap of 3.39 eV[10–13] and, close in value to that of the exciton E_C band,[13] the 2.94 eV is consistent with the value we have observed here as 2.96 eV and should correspond to the direct allowed electronic transitions which are also known as the E_A band. These two peaks are also observed for Ga_2S_3 coated onto glass substrates and are not shifted by using the Ge substrate. On the other hand, the dielectric resonance peaks which appeared at 2.30 eV and at 1.32 eV for Ga_2S_3 coated onto glass appear here at 2.25 eV and at 1.47 eV, respectively. The 2.25 eV peak is very close to that observed as the optical gap (2.48 eV) for the hexagonal β-Ga_2S_3 polycrystals.[10–13] The peak which appeared at 1.47 eV is mainly attributed to the defects which exist in the

Table I. Valence band offset for Ge-based heterojunctions as reported in Ref. 23

Heterojunction	$\lvert\Delta E_g\rvert$ (eV)
Ge/Ga_2S_3	0.82[a]
CdTe/Ge	0.85
CdS/Ge	0.80
CdTe/Ge	0.85
GaP/Ge	0.80

[a]Current work.

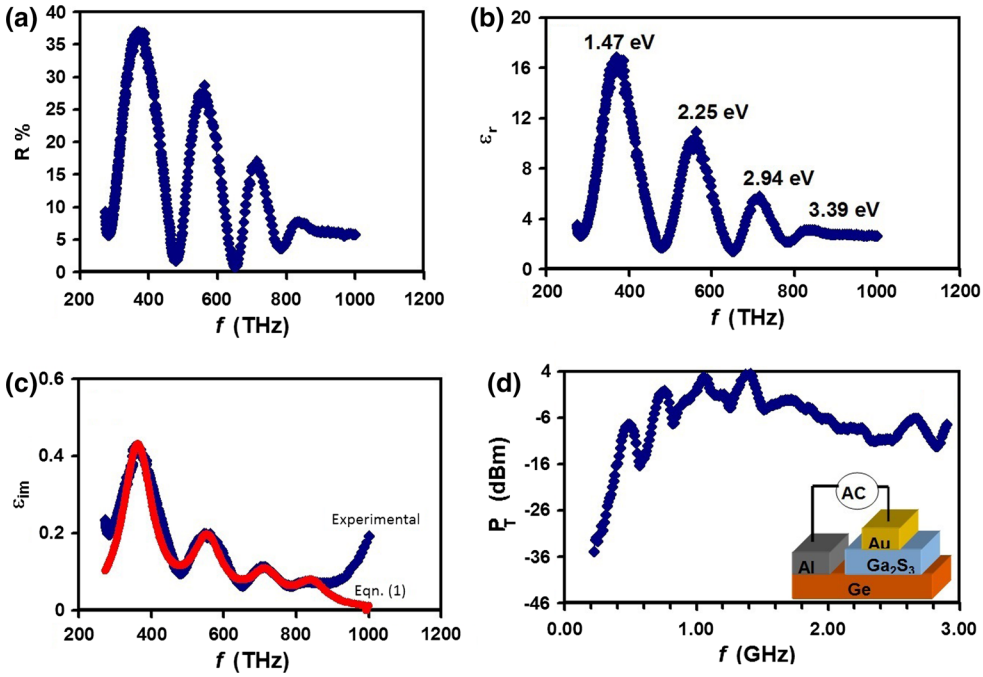

Fig. 4. (a) The reflectance spectra and (b) the real part and (c) the imaginary part of the dielectric spectra for the Ge/Ga_2S_3 interface. The red color which appears in (c) shows the fitting of Eq. 2. (d) The transmitted power spectra of the GE/Ga_2S_3 interface (Color figure online).

structure of the Ge and Ge/Ga_2S_3 interface. The defects which are also accepted to arise from dislocations and exhibited a density of 2.15×10^{12} points/cm^2 as determined from Fig. 2b create interbands which lead to interband transitions in the energy band gap of the Ga_2S_3. These defects are usually formed on the c-plane along the a-axis and are assigned to the Ga and S vacancies.[13]

Consistent with the real part of the dielectric constant, the ε_{im} spectra which are shown in Fig. 4b also displayed resonance peaks centered at 819 (3.37 eV), 700 (2.89 eV), 545 (2.24 eV) and 350 THz (1.44 eV). The shift in the value of the peaks as compared to those determined from the ε_r spectra is mainly due to the phase changes that happen to the incident light waves. To explore the plasmon–electron dynamics at the surface of Ge due to the Ga_2S_3 interfacing, the imaginary part of the dielectric constant is modeled in accordance with the Drude–Lorentz theory which presents the dielectric constant spectra through the relationship,[25]

$$\varepsilon_{\text{im}} = \sum_{i=1}^{k} \frac{w_{pe_i}^2 w}{\tau_i \left(\left(w_{e_i}^2 - w^2 \right)^2 + w^2 \tau_i^{-2} \right)}. \qquad (2)$$

In this equation, τ, $w_{pe} = \sqrt{4\pi n e^2 / m*}$, w_e, n and $m*$ are the free electrons scattering time, the electron-bounded plasma frequency, the reduced resonant frequency, the free electron density, and the effective mass of free carriers after the heterojunction is created, repectively. The drift mobility of electrons which results from the incident electromagnetic field can also be determined from the relationship, $\mu = e\tau/m*$. The Drude–Lorentz model assumes that the coupled oscillations which appear in the dielectric spectra arise from the oscillation of free electrons with respect to positive ions (plasmon). The electron-bounded plasmon resonance which is the resonant oscillation of conduction electrons at the interface between the two dielectrics which exhibit positive and negative permittivities is usually excited by light waves. The maxima in the dielectric spectra appear when the frequency (w) of the incident light wave matches the natural frequency of the free surface electrons (w_e). The surface free electrons which oscillate against the restoring force of positive nuclei cease when the energy is lost in the resistance (electronic friction) as a damping force of coefficient = τ^{-1}.

The computed data with the help of the above-mentioned equation appear as red colored, as plotted in Fig. 4b. The fitting is actualized with the parameters which are reported in Table II, assuming the effective mass of holes in Ge to be $0.38m_o$[12] and effective mass of electrons in Ga_2S_3 to be $0.40m_o$[26] $m_e^* = (m_{Ge}^{*-1} + m_{Ga2S3}^{*-1})^{-1} = 0.19m_o$. The tabulated parameters provide information about the electronic motion and plasmon–electron coupled resonance at Ge/Ga_2S_3 interface. As seen from the table, while the scattering time of electrons remains constant in all the studied frequency range of terahertz frequency, indicating a constant damping coefficient, the reduced resonant frequency (w_e) increases and the electron-bounded plasma frequency (w_{pe}) decreases with the increasing number of oscillators (k = 1–4). The decrease in these values is associated with the

Table II. The fitting parameters of the plasmon–electron interactions at the Ge/Ga_2S_3 interface

i	τ_i (fs)	w_{ei} ($\times 10^{15}$ Hz)	n ($\times 10^{18}$ cm^{-3})	μ (cm^2/Vs)	w_{pei} (GHz)
1	1.6	2.3	2.7	15.61	2.30
2	1.6	3.5	1.6	15.61	1.77
3	1.6	4.5	1.0	15.61	1.40
4	1.6	5.3	0.9	15.61	1.33

decrease in the free carrier density (n). The latter is ascribed to the increased electron–hole recombinations at the interface.[27,28] The increase in the reduced resonant frequency (w_e), which takes into account the effects of the local fields (interband transitions) on the dielectric function with increasing incident light frequency, may be ascribed to the lesser effect of the interband transitions owing to higher photon energies that can pick up electron–hole pairs from the valence band directly to the conduction band.[25–28]

An interesting property of the computed parameters for the Ge/Ga_2S_3 interface is the behavior of the drift mobility which exhibits a relativity high and constant value of 15.61 cm^2/Vs. This value, which is close to that reported as 16 cm^2/Vs[12] for n-type GaS, indicates the highly stable performance of the Ge/Ga_2S_3 interface. The value of the drift mobility nominates the p–n junction for use as thin film transistors being able to carry dual duties like microwave trapping and optoelectronic applications.[29] On the other hand, the electron-bounded plasma frequencies are of gigahertz levels, indicating that, if a microwave propagates through the Ge/Ga_2S_3 interface, it can penetrate only if its frequency is higher than w_{pe}, otherwise, the signal is reflected back. Since the computed w_{pe} values are in the range of 2.30–1.33 GHz, then the Ge/Ga_2S_3 interface can be employed as wave traps of at least four resonant frequencies which suits microwave communications. To verify this result, a wave form signal of average powers of ~4.0 dBms (2.5 mW) was imposed on the device terminals which are shown in the inset of Fig. 4d. The signal frequency was in the range of 0.2–2.5 GHz. The output power spectra of the transmitted power (T_p) are shown in Fig. 4d. As readable from the figure, with increasing incident wave frequency, the transmitted wave power increases. In particular, while the T_p value is −34.85 dBm (0.33 μW) at 0.22 GHz, it increases to 2.3 dBm (1.7 mW) and to 4.0 dBm (2.5 mW) when f reaches 1.1 GHz and 1.41 GHz, respectively. The numerical values suggest that the wave transitivity which was less than 0.1% at 0.22 GHz increases to 68.0% and to 100% at 1.1 GHz and 1.41 GHz, respectively. The ability of the incident ac signal wave to transmit through the Ge/Ga_2S_3 interface is in accordance with the computed plasmon frequencies which are then ascribed to the plasmon–electron coupling at the interface. The tested wave transitivity through the device confirms the ability of the electron–plasmon coupling to control the interface performance.

CONCLUSIONS

We have discussed the design and characterization of a promising heterojunction which is made of two polycrystalline Ge and Ga_2S_3 thin layers. The properties of the Ge/Ga_2S_3 interface were explored by means of SEM, EDX , XRD, Raman spectroscopy, visible light spectrophotometery and ac signal spectroscopy which indicated that the good lattice match which leads to relatively low strain allowed the creation of equal conduction and valence band offsets at the Ge/Ga_2S_3 interface. The interface behaved as an ideal electron–plasmon resonator that transmits waves of frequencies above 1.3 GHz. Thus, in addition to the dielectric resonance peaks which are observed above 350 THz, the device could behave as a wave trap for all waves in the range of 0.2–1.3 GHz.

ACKNOWLEDGEMENTS

This project was funded by the Deanship of Scientific Research (DSR), at King Abdulaziz University, Jaddah, under the Grant Number G-229-363-37. The authors, therefore, acknowledge with thanks the DSR technical and financial support.

REFERENCES

1. Z. Zhang, W. Wang, L. Wang, and S. Sun, *ACS Appl. Mater. Interface* 4, 593 (2012).
2. H.D. Kim, H. Ohkita, H. Benten, and Sh. Ito, *ACS Appl. Mater. Interface* 6, 17551 (2014).
3. C. Liu, K. Wang, X. Gong, and A.J. Heeger, *Chem. Soc. Rev.* 45, 4825 (2016).
4. J.W. Jung, J.W. Jo, E.H. Jung, and W.H. Jo, *Organ. Electron.* 31, 149 (2016).
5. S.E. Al Garni and A.F. Qasrawi, *Phys. Stat. Sol. (a)* 212, 1845 (2015).
6. Y.-C. Yeo, X. Gong, M.J.H. Van Dal, G. Vellianitis, and M. Passlack, *IEEE International Electron Devices Meeting (IEDM)* (2015).
7. Z. Huang, J-G. Huang, K.A. Kokh, V.A. Svetlichnyi, A.V. Shabalina, Yu.M. Andreev, and G.V. Lanskii, *40th International Conference on Infrared, Millimeter, and Terahertz waves (IRMMW-THz)* (2015).
8. P. Blood, *Quantum Confined Laser Devices: Optical Gain and Recombination in Semiconductors*, Vol. 23 (Oxford: Oxford Univerity Press, 2015).
9. H.W. Chiu, C.N. Chervin, and S.M. Kauzlarich, *Chem. Mater.* 17, 4858 (2005).
10. H.F. Liu, K.K.A. Antwi, N.L. Yakovlev, H.R. Tan, L.T. Ong, S.J. Chua, and D.Z. Chi, *ACS Appl. Mater. Interface* 6, 3501 (2014).

11. C. Lin, G. Qu, Zh Li, Sh Dai, H. Ma, T. Xu, Q. Nie, and X. Zhang, *J. Am. Ceram. Soc.* 96, 1779 (2013).
12. O. Madelung, *Semiconductors: Data Handbook* (New York: Springer, 2012).
13. C.-H. Ho and H.-H. Chen, *Sci. Rep.* 4, 6143 (2014).
14. S.E. Al Garni and A.F. Qasrawi, *J. Alloys Compd.* 633, 499 (2015).
15. J.J. Sheng, D. Leonhardt, S.M. Han, S.W. Johnston, J.G. Cederberg, and M.S. Carroll, *J. Vac. Sci. Technol. B* 31, 051201 (2013).
16. J. Liu, C. Liang, Zh Tian, Sh Zhang, and G. Shao, *Sci. Rep.* 3, 1741 (2013).
17. R.K. Dukor, J.M. Chalmers, and P.R. Griffiths, *Handbook of Vibrational Spectroscopy, Vibrational Spectroscopy in the Detection of Cancer* (New York: Wiley, 2001).
18. G. Job and R. Rüffler, *Physical Chemistry from a Different Angle* (Switzerland: Springer, 2016).
19. V. Stevanović, S. Lany, X. Zhang, and A. Zunger, *Phys. Rev. B* 85, 115104 (2012).
20. C. Lin, L. Calvez, H. Tao, M. Allix, A. Moréac, X. Zhang, and X. Zhao, *J. Solid State Chem.* 184, 584 (2011).
21. N. Seeburrun, E.F. Archibong, and P. Ramasami, *Chem. Phys. Lett.* 467, 23 (2008).
22. L. Makinistian and E.A. Albanesi, *Phys. Rev. B* 74, 045206 (2006).
23. M.C. Turcu, *Defect Energies, Band Alignments, and Charge Carrier Recombination in Polycrystalline Cu* (*In*, *Ga*)(*Se*, *S*)$_2$ *Alloys* (2003). http://www.qucosa.de/recherche/frontdoor/?tx_slubopus4frontend%5Bid%5D=1146.
24. S.E. Al Garni and A.F. Qasrawi, *Mater. Sci. Semicond. Process.* 31, 678 (2015).
25. G. Dresselhaus and M.S. Dresselhaus, Optical properties of solids, in *Proceedings of the International School of Physics*, ed. by E. Fermi, J. Tauc (New York: Academic, 1966).
26. S.R. Alharbi and A.F. Qasrawi, *Plasmonics* (2016). doi: 10.1007/s11468-016-0357-4.
27. L.A. Sinatra, P. LaGrow, W. Peng, A.R. Kirmani, A. Amassian, H. Idriss, and O.M. Bakr, *J. Catal.* 322, 109 (2015).
28. L.P.K. Riuttanen, O. Svensk, J. Oksanen, and S. Suihkonen, *Appl. Phys. Lett.* 107, 051106 (2015).
29. X. Xu, T. Xiao, X. Gu, X. Yang, S.V. Kershaw, N. Zhao, J. Xu, and Q. Miao, *ACS Appl. Mater. Interface* 7, 28019 (2015).